



Research Article

Magneto-double-diffusive convection in a hybrid nanofluid

Monal BHARTY¹, Atul K. SRIVASTAVA^{2,*}, Hrishikesh MAHATO¹

¹Department of Mathematics, Central University of Jharkhand, Ranchi, Jharkhand, 835205, India

²Department of Mathematics, AIAS, Amity University Jharkhand, Ranchi, Jharkhand, 835103, India

ARTICLE INFO

Article history

Received: 17 November 2023

Revised: 15 January 2024

Accepted: 26 July 2024

Keywords:

Brownian Motion; External
Magnetic Field; Hybrid
Nanofluid; Rayleigh Number;
Stability Analysis

ABSTRACT

From an experimental as well as an industrial perspective, hybrid nanofluids are crucial to the advancement of the thermal properties of pure fluid. Contrary to one nanoparticle for top-heavy dispersion and solute gradient, which aids in early convection in a lower heated nanofluid layer, the combination of two different types of nanoparticles in the base liquid reduces the stationary state convection. While earlier research looked at the linear stability analysis of double diffusive convection in hybrid nanofluid without accounting for magnetic field, this work investigates the effect of magnetic field on the onset of double diffusive convection in hybrid nanofluid. In this paper, we give a comparative analysis of four boundary combinations. For both realistic (i.e., Rigid-Rigid (R/R), Rigid-Free (R/F), Free-Rigid (F/R)) and non-realistic (i.e., Free-Free (F/F)) boundary surfaces, the analytical and numerical solutions are derived. Here, an analysis of linear stability is conducted using the normal mode technique. For three different types of boundary conditions (R/R, F/R, and R/F), the ensuing eigenvalue problem is solved using the Galerkin technique; in the instance of F/F, an exact solution is obtained. The effects of various parameters on stationary convection under various boundary conditions are depicted graphically and explained theoretically. With an increase in the value of Chandrasekhar number (Q), the stability of the system also increases for all four boundary combinations (i.e., R/R, R/F, F/R, and F/F). The stability of the system decreases with an increasing value of the thermo-nanofluid Lewis number (Ln_1) and nanoparticle concentration numbers (Rn_1 , Rn_2). With an increasing value of Ln_2 , the system becomes stable for R/R and F/R boundaries, whereas it becomes unstable for F/F and R/F boundaries.

Cite this article as: Bharty M, Srivastava AK, Mahato H. Magneto-double-diffusive convection in a hybrid nanofluid. Sigma J Eng Nat Sci 2025;43(4):1166–1178.

INTRODUCTION

Fluids that are frequently employed as efficient heat transfer media include water, ethylene glycol, and motor oil. These fluids are not very suitable as heat transfer fluids because of their lower thermal conductivity. It is, however, naturally

preferable to mix metals with fluids to create a heat transfer medium that functions like a fluid but has the thermal conductivity of a metal because metals have three times the thermal conductivity of fluids [1]. In nanofluid, which [2] initially described, non-micrometer-sized particles are scattered

*Corresponding author.

*E-mail address: atulshaswat@gmail.com, aksrivastava@rnc.amity.edu

This paper was recommended for publication in revised form by
Editor-in-Chief Ahmet Selim Dalkilic



throughout the host (base) fluid. A larger thermal conductivity enhancement can be obtained if a base fluid with lower thermal conductivity is utilized, as demonstrated by [3]. The physical and thermal properties of nano-metal particles and the base liquid have a significant impact on the behavior of nanofluid. Four types of nanofluid are distinguished based on the type of nanoparticles: metal, metal oxide, carbon, and metal hybrid. The host (base) fluids that are commonly used to produce nanofluids are ethylene glycol, methanol, water, and oils. Nanofluids have a wide range of applications in the automotive sector (including hybrid and internal combustion engines), air conditioning, solar and power plant cooling, nuclear reactors, space and defense systems, and pharmaceutical processes. As a result, in recent years, interest in oil-based nanofluids, including carbon nanotubes, TiO₂, CuO, Al₂O₃, AlN, and SiO₂, for industrial and engineering applications has increased [4-6]. Using the two-phase model [7, 8], quantitatively investigated natural and mixed convection heat transfers in a nanofluid within a square cavity. They found that the nanoparticle distribution is non-uniform for low Rayleigh and high Richardson numbers and that thermophoretic effects are minimal for nanoparticles with high thermal conductivity. They also concluded that the use of homogeneous and single-phase models is suitable in such circumstances. By taking into account Newtonian and non-Newtonian nanofluids with and without dusty particles, [9, 10] were able to determine the prerequisites for the existence of stationary and oscillatory convections in such nanofluids in the presence or absence of a porous medium. There has been a lot of research done on nanofluids in recent years, including research on their preparation, characterization, modeling, convective and boiling heat transfer, and applications. These are due to their unique properties, which include excellent load-carrying capacity, extreme pressure, and friction-reducing qualities [11]. However, hybrid nanofluids are a new class of nanofluids that can be made by suspending (i) different types of nanoparticles (two or more types) in base fluid and (ii) hybrid (composite) nanoparticles in base fluid. A hybrid material is something that simultaneously combines the physical and chemical properties of many materials and offers these properties in a homogeneous form. Amazing physicochemical properties that do not exist in the separate components can be found in synthetic hybrid nanomaterials. The properties of these composites have been extensively studied [12], and hybrid materials containing carbon nanotubes (CNTs) have been applied in nanocatalysts, electrochemical sensors, biosensors, and other applications [13]. Ahmad, [14] imposed Cu-Al₂O₃ nanoparticles and water as the base fluid to study the mixed convection flow of the hybrid nanofluid over a nonlinear stretching sheet. This research shows that the temperature of the hybrid nanofluid rises in response to thermal radiation, but its velocity falls in the presence of a magnetic field. However, the application of these hybrid nanomaterials in nanofluids has not yet been identified. There has been very little work done on hybrid nanofluids, and there is still a lot of research being done.

Double diffusive convection of hybrid nanofluids is examined by [15]. Double-diffusive convection in flow has various applications, and it is widely employed in many natural and experimental systems where mass and heat diffusion occur simultaneously. The fluid motion is produced by the simultaneous diffusion of two factors, namely temperature and concentration variations, which result in buoyancies. As a result, this phenomenon in flow is known as double-diffusive convection [16]. The fluid density is significantly influenced by the solute gradient and heat, and as a result, these linked phenomena can create unique flow behavior even in fluids with a uniform density distribution. Double diffusion in the naturally convective flow of water-based fluid saturated in a corrugated enclosure and containing hybrid nanoparticles composed of copper (Cu) and alumina (Al₂O₃) is examined by [17]. Sharma and Gupta [18] took into account the heat and solute transport in a rotating nanofluid with a porous, below-heated layer. According to their research, the coriolis force term caused by rotation stabilizes the system; however, the Darcy number causes the layer to become unstable or stable depending on the wave number, which can be small or big. In their study, Pranesh et al. [19] looked at the convection that occurs in water when three diffusing components are added. They discovered in their investigation that the best estimates of the thermophysical properties of the aqueous solutions serve as the foundation for the critical values of the Rayleigh, Nusselt, and Sherwood numbers. [20-22] evaluated the coupled effect of Hall and heat transport on the MHD flow in different fluids. The Hall impact on a vertical porous Jeffrey fluid flow with a magnetic field was also explored by [20].

What happens when we look at how an external magnetic field interacts with double diffusive convection in hybrid nanofluid? Due to its engineering applications in crystal formation in liquids, geophysics, geothermal reservoirs, etc., convective heat transfer associated with magnetic field impact has gained interest recently [23, 24]. Numerous studies have looked at how different configurations and circumstances affect convective heat transport when subjected to external magnetic fields. Using the shooting method, [25] investigated magnetohydrodynamic Casson fluid flow over a deformable porous channel and found that the influence of the magnetic field and Casson parameters reduced the fluid velocity and particle displacement. By using the symmetrical finite volume method, [26] investigated magnetized nanofluid flow in a symmetrical E-shaped chamber in the presence of an inclined magnetic field. They discovered that the increase in Richardson number increased the heat transfer rate, while the magnetic field effect decreased flow circulation. In the presence of a magnetic field applied at an angle to the horizontal axis, Roy, [27] investigated the natural convective flow and heat transfer of a hybrid nanofluid confined in an enclosure with several heat sources at the bottom wall. A magnetized Ag-MgO water hybrid nanofluidic stream inside a cube-shaped enclosure with an inner circular cylinder installed inside the

cube is computationally investigated by [28]. According to this study, the magnetic factor lowers energy transmission, whereas the Rayleigh number increases it. High heat transference is revealed by the cold mode of the cylinder, whereas high velocity magnitudes within the cube are explored by the hot mode. For steady two-dimensional and incompressible flow with a convective boundary condition in a curved-coordinate porous system with ohmic heating, Rashad [29] examined the variation of heat on the MHD Williamson hybrid nanofluid (Ag-TiO₂/H₂O) model. This study found that while convective boundary conditions and thermal radiation increase surface friction, growing permeability, Biot, and Eckert numbers enhance temperature profiles while reducing heat transfer. In 2024, Anee et al. [30] presented the study for analysing the magnetohydrodynamic convective heat transport of hybrid nanofluids in a chamber with multiple heaters (such as hot microchips). They used the multiple-relaxation-time, lattice Boltzmann method and graphics processing unit computing for analysing their work. The radiative magnetohydrodynamic (MHD) mixed convective alumina-copper/water hybrid nanofluid flow via an angled shrinking plate was also studied by Wahid et al. [31]. Their research shed important light on basic transport phenomena as the movement of mass, momentum, or heat.

Taking motivation from Pundir's recent work [15], we are interested in understanding the influence of magnetic field on hybrid nanofluid double diffusive convection since the aforementioned study does not account for magnetic field, which is presently having a lot of practical applications. The outline of the paper is as follows: We provide a brief mathematical model of the physical situation in Section 2. In Section 3, linear stability analysis for both realistic and non-realistic boundary conditions is provided. In Section 4, findings and discussion are presented. The analysis ends with a few key points in Section 5.

MATHEMATICAL FORMULATION OF THE PROBLEM

An unbounded horizontal layer of hybrid nanofluid of thickness d is considered between the perfectly insulating planes located at $z^* = 0$ and $z^* = d$ under the influence of an externally imposed constant magnetic field. At the lower plane ($z^* = 0$) and higher plane ($z^* = d$), the temperature is assumed $T_0^* + \Delta T^*$ and T_0^* respectively with $\Delta T^* \ll T_0^*$. Also, at the lower plane ($z^* = 0$) and, higher plane ($z^* = d$), the concentrations are assumed $C_0^* + \Delta C^*$ and C_0^* respectively. In this analysis, astrisks represent the dimensional variables, and non-dimensional variables are exclusive of astrisks. Here, the gravitational force is taken as $g\hat{k}$. The temperature and concentration changes in nanofluid are assumed to be very small. It is assumed the nanofluid mixture is uniform and in a local thermal symmetrical state. To linearize the mathematical equations, the Oberbeck-Boussinesq hypothesis has been used. Also, for the mathematical formulation, we have taken into account that

- (i) Newtonian flow is regarded as laminar, and the nanofluid under consideration is incompressible.
- (ii) The nanoparticles are being perched in the base liquid using either surface charge technology or surfactant, preventing the hoard so that the nanoliquids are stable.
- (iii) During the convection, there is no chemical reactions take place. The base liquid phase and both types of nanoparticles are symmetrical with respect to temperature. Also, the thermo-physical ability of nanofluid is fixed (Boussinesq Hypothesis).
- (iv) Size matters in making nanofluids with novel properties, so in this study, the spherical nano-particles are measured. Radioactive heat transport is not considered as it is exceptionally small.

The principle equations of conservation that characterize the flow of a hybrid nanofluid layer in dimensional form are as follows [15] and [32] :-

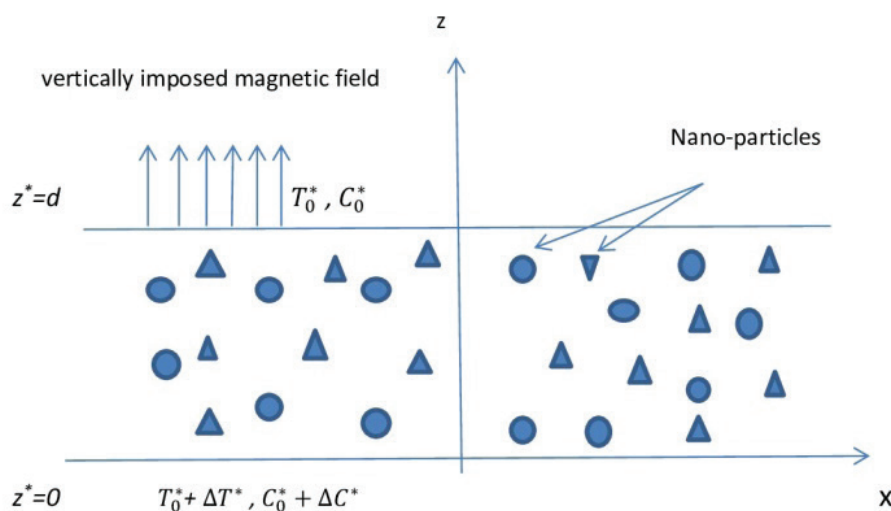


Figure 1. Schematic diagram of the problem considered.

$$\nabla \cdot \mathbf{u}^* = 0, \tag{1}$$

$$\nabla \cdot \mathbf{H}^* = 0, \tag{2}$$

$$\rho \left((\mathbf{u}^* \cdot \nabla^*) \mathbf{u}^* + \frac{\partial \mathbf{u}^*}{\partial t^*} \right) - \mu_m (\mathbf{H}^* \cdot \nabla) \mathbf{H}^* = -\rho g \hat{\mathbf{k}} - \nabla^* p^* + \mu \nabla^{*2} \mathbf{u}^*, \tag{3}$$

$$\frac{\partial \mathbf{H}^*}{\partial t^*} + \mathbf{u}^* \cdot \nabla \mathbf{H}^* - \mathbf{H}^* \cdot \nabla^* \mathbf{u}^* = \Lambda \nabla^{*2} \mathbf{H}^*, \tag{4}$$

$$(\rho c)_f \left((\mathbf{u}^* \cdot \nabla^*) T^* + \frac{\partial T^*}{\partial t^*} \right) = \kappa \nabla^{*2} T^* + (\rho c)_{p1} [D_{B1} \nabla^* \phi_1^* \cdot \nabla^* T^* + (D_{T1}/T_0^*) \nabla^* T^* \cdot \nabla^* T^*] + (\rho c)_{p2} [D_{B2} \nabla^* \phi_2^* \cdot \nabla^* T^* + \left(\frac{D_{T2}}{T_0^*} \right) \nabla^* T^* \cdot \nabla^* T^*], \tag{5}$$

$$\frac{\partial C^*}{\partial t^*} + (\mathbf{u}^* \cdot \nabla^*) C^* = D_S \nabla^{*2} C^*, \tag{6}$$

$$\frac{\partial \phi_1^*}{\partial t^*} + (\mathbf{u}^* \cdot \nabla^*) \phi_1^* = D_{B1} \nabla^{*2} \phi_1^* + \left(\frac{D_{T1}}{T_0^*} \right) \nabla^{*2} T^*, \tag{7}$$

$$\frac{\partial \phi_2^*}{\partial t^*} + (\mathbf{u}^* \cdot \nabla^*) \phi_2^* = D_{B2} \nabla^{*2} \phi_2^* + \left(\frac{D_{T2}}{T_0^*} \right) \nabla^{*2} T^*. \tag{8}$$

In the Boussinesq hypothesis, the density equation is

$$\rho_f = \rho_{f0} [1 - \beta_T (T^* - T_0^*) - \beta_C (C^* - C_0^*)],$$

also,

$$\rho = \phi_1^* \rho_{p1} + \phi_2^* \rho_{p2} + (1 - \phi_1^* - \phi_2^*) \rho_f.$$

Here ρ_{p1} , ρ_{p2} and ρ_f are the nanoparticles mass densities and base fluid density. We obtain

$$\rho = \phi_1^* \rho_{p1} + \phi_2^* \rho_{p2} + (1 - \phi_1^* - \phi_2^*) \rho_{f0} [1 - \beta_T (T^* - T_0^*) - \beta_C (C^* - C_0^*)].$$

Since the volumetric fraction of nanoparticles is small, taking the density of the base fluid as that of the density of nanofluid i.e. $\rho \cong \rho_{f0}$ as adopted by [32], the specific weight becomes

$$\rho g \cong \phi_1^* \rho_{p1} + \phi_2^* \rho_{p2} + (1 - \phi_1^* - \phi_2^*) \rho [1 - \beta_T (T^* - T_0^*) - \beta_C (C^* - C_0^*)] g. \tag{9}$$

Here, the velocity of the nanofluid layer is taken as $\mathbf{u}^* = (u^*, v^*, w^*)$; T^* (°K) is the nanofluid temperature; β_T (°K) is the thermal volumetric coefficient; ϕ_1^* , ϕ_2^* are the nanoparticle volume fractions; $\mathbf{H}^* = (H_x^*, H_y^*, H_z^*)$ is Magnetic field; μ (N s/m²) is the viscosity; D_{B1} , D_{B2} (m²/s) are the Brownian diffusion coefficients; D_{T1} , D_{T2} (m²/s) are the thermophoretic diffusion coefficients; D_S (m²/s) is the solutal diffusivity. Also, we have assumed that the solute concentration and nanoparticle volume fractions are fixed at the boundaries. Now the boundary conditions are defined as:

$$\begin{aligned} w^* = 0, \quad \frac{\partial w^*}{\partial z^*} + \lambda_1 d \frac{\partial^2 w^*}{\partial z^{*2}} = 0, \quad T^* = T_0^* + \Delta T^*, \\ C^* = C_0^* + \Delta C^*, \quad \phi_1^* = \phi_{10}^*, \quad \mathbf{H}^* \times \hat{\mathbf{k}} = 0, \\ \phi_2^* = \phi_{20}^* \quad \text{at } z^* = 0, \end{aligned} \tag{10}$$

$$\begin{aligned} w^* = 0, \quad \frac{\partial w^*}{\partial z^*} - \lambda_2 d \frac{\partial^2 w^*}{\partial z^{*2}} = 0, \quad T^* = T_0^*, \quad C^* = C_0^*, \\ \phi_1^* = \phi_{11}^*, \quad \mathbf{H}^* \times \hat{\mathbf{k}} = 0, \quad \phi_2^* = \phi_{21}^* \quad \text{at } z^* = d. \end{aligned} \tag{11}$$

Here d stands for the width of the layer. For the case of rigid boundaries, the parameters λ_1 and λ_2 taken to have a zero value, and for the case of a free boundary, the values of the parameters are infinity.

Now, introduce the non-dimensional variables

$$\begin{aligned} (x, y, z), \phi_1, \phi_2, p, T, (u, v, w), t \text{ and } C \text{ is defined as} \\ (x, y, z) = \frac{(x^*, y^*, z^*)}{d}, \quad \phi_1 = \frac{(\phi_1^* - \phi_{10}^*)}{(\phi_{11}^* - \phi_{10}^*)}, \quad \phi_2 = \frac{(\phi_2^* - \phi_{20}^*)}{(\phi_{21}^* - \phi_{20}^*)}, \quad p = \frac{p^* d^2}{\mu \alpha_f}, \\ T = \frac{(T^* - T_0^*)}{\Delta T^*}, \quad (u, v, w) = \frac{d(u^*, v^*, w^*)}{\alpha_f}, \quad t = \frac{\alpha_f t^*}{d^2}, \quad C = \frac{(C^* - C_0^*)}{\Delta C^*}, \quad \mathbf{H} = \frac{\mathbf{H}^*}{H_b}. \end{aligned}$$

The non-dimensional form of Eqn. (1)–(8) is

$$\nabla \cdot \mathbf{u} = 0, \tag{12}$$

$$\nabla \cdot \mathbf{H} = 0, \tag{13}$$

$$\begin{aligned} \frac{1}{Pr} \left(\frac{\partial \mathbf{u}}{\partial t} + (\mathbf{u} \cdot \nabla) \mathbf{u} \right) = QPm (\mathbf{H} \cdot \nabla) \mathbf{H} - \nabla p + \nabla^2 \mathbf{u} + \frac{Rs}{Le} C \hat{\mathbf{e}}_z \\ - Rn_1 \phi_1 \hat{\mathbf{e}}_z - Rn_2 \phi_2 \hat{\mathbf{e}}_z + RaT \hat{\mathbf{e}}_z - Rm \hat{\mathbf{e}}_z, \end{aligned} \tag{14}$$

$$\frac{\partial \mathbf{H}}{\partial t} + \mathbf{u} \cdot \nabla \mathbf{H} - \mathbf{H} \cdot \nabla \mathbf{u} = Pm \nabla^2 \mathbf{H}, \tag{15}$$

$$\begin{aligned} \frac{\partial T}{\partial t} + (\mathbf{u} \cdot \nabla) T = \frac{NB_1}{Ln_1} \nabla \phi_1 \cdot \nabla T + \frac{NA_1 NB_1}{Ln_1} \nabla T \cdot \nabla T \\ + \frac{NB_2}{Ln_2} \nabla \phi_2 \cdot \nabla T + \frac{NA_2 NB_2}{Ln_2} \nabla T \cdot \nabla T + \nabla^2 T, \end{aligned} \tag{16}$$

$$\frac{\partial C}{\partial t} + (\mathbf{u} \cdot \nabla) C = \frac{1}{Le} \nabla^2 C, \tag{17}$$

$$\frac{\partial \phi_1}{\partial t} + (\mathbf{u} \cdot \nabla) \phi_1 = \frac{1}{Ln_1} \nabla^2 \phi_1 + \frac{NA_1}{Ln_1} \nabla^2 T, \tag{18}$$

$$\frac{\partial \phi_2}{\partial t} + (\mathbf{u} \cdot \nabla) \phi_2 = \frac{1}{Ln_2} \nabla^2 \phi_2 + \frac{NA_2}{Ln_2} \nabla^2 T. \tag{19}$$

The dimensionless boundary conditions take the form:-

$$w = 0, \quad \frac{\partial y}{\partial x} + \lambda_1 \frac{\partial^2 w}{\partial z^2} = 0, \quad \phi_1 = 0, \quad \phi_2 = 0, \quad T = 1, \quad C = 1 \quad \text{at } z = 0, \tag{20}$$

$$w = 0, \quad \frac{\partial y}{\partial x} - \lambda_2 \frac{\partial^2 w}{\partial z^2} = 0, \quad \phi_1 = 1, \quad \phi_2 = 1, \quad T = 0, \quad C = 0 \quad \text{at } z = 1. \tag{21}$$

The non-dimensional parameters are; Chandrashekhara number ($Q = \frac{\mu_m H_b^2}{\Lambda \mu}$); the Prandtl number ($Pr = \frac{\mu}{\rho \alpha_f}$); the temperature-based Rayleigh number ($Ra = \frac{\rho g \beta_T d^3 \Delta T^*}{\mu \alpha_f}$); the concentration-based Rayleigh number ($Rs = \frac{\rho g \beta_C d^3 \Delta C^*}{\mu D_S}$); the density-based Rayleigh number ($Rm = [\rho_{p_1} \phi_{10}^* + \rho_{p_2} \phi_{20}^* - \rho(1 - \phi_{10}^* - \phi_{20}^*)] \frac{g d^3}{\mu \alpha_f}$); the nanoparticles concentration Rayleigh numbers ($Rn_1 = \frac{[(\rho_{p_1} - \rho)(\phi_{11}^* - \phi_{10}^*)](g d^3)}{\mu \alpha_f}$) and ($Rn_2 = \frac{[(\rho_{p_2} - \rho)(\phi_{21}^* - \phi_{20}^*)](g d^3)}{\mu \alpha_f}$); magnetic prandtl number ($Pm = \frac{\Lambda}{\alpha_f}$); the Lewis number ($Le = \frac{\alpha_f}{D_S}$); the modified diffusivity ratios ($N_{A_1} = \frac{D_{T_1} \Delta T^*}{D_{B_1} T_0^* (\phi_{11}^* - \phi_{10}^*)}$) and ($N_{B_1} = \frac{(\rho c) p_1 (\phi_{21}^* - \phi_{20}^*)}{\rho c}$). The terms containing the product of ϕ_1 and ϕ_2 with T are neglected to linearization the equations.

LINEAR STABILITY ANALYSIS

Basic State

The basic state of present problem expressed as:-

$$\begin{aligned} \mathbf{u} &= \mathbf{0}, p = p_b(z), \phi_1 = \phi_{1b}(z), \phi_2 = \phi_{2b}(z), \\ T &= T_b(z), C = C_b(z), \mathbf{H} = \mathbf{H}_b(z). \end{aligned} \tag{22}$$

Using (22), Eqn. (12)-(19) take the form:-

$$\begin{aligned} QPm \mathbf{H}_b \frac{d}{dz} \mathbf{H}_b - \frac{d}{dz} p_b - Rn_1 \phi_{1b} - Rn_2 \phi_{2b} + Ra T_b \\ + \frac{Rs}{Le} C_b - Rm = 0, \end{aligned} \tag{23}$$

$$Pm \frac{d^2}{dz^2} \mathbf{H}_b = 0, \tag{24}$$

$$\begin{aligned} \frac{d^2 T_b}{dz^2} + \frac{N_{B_1}}{Ln_1} \left(\frac{d\phi_{1b}}{dz} \cdot \frac{dT_b}{dz} \right) + \frac{N_{A_1} \cdot N_{B_1}}{Ln_1} \left(\frac{dT_b}{dz} \right)^2 \\ + \frac{N_{B_2}}{Ln_2} \left(\frac{d\phi_{2b}}{dz} \cdot \frac{dT_b}{dz} \right) + \frac{N_{A_2} \cdot N_{B_2}}{Ln_2} \left(\frac{dT_b}{dz} \right)^2 = 0, \end{aligned} \tag{25}$$

$$\frac{d^2 C_b}{dz^2} = 0, \tag{26}$$

$$\frac{d^2 \phi_{1b}}{dz^2} + N_{A_1} \frac{d^2 T_b}{dz^2} = 0, \tag{27}$$

$$\frac{d^2 \phi_{2b}}{dz^2} + N_{A_2} \frac{d^2 T_b}{dz^2} = 0. \tag{28}$$

Boundary conditions becomes:-

$$\begin{aligned} \phi_{1b}(0) = 0, \phi_{2b}(0) = 0, T_b(0) = 1, C_b(0) = 1, \phi_{1b}(1) = 1, \\ \phi_{2b}(1) = 1, T_b(1) = 0 \text{ and } C_b(1) = 0. \end{aligned} \tag{29}$$

Infrequently cases of nanofluid layers, $\frac{Ln_1}{\phi_{11}^* - \phi_{10}^*}$ and $\frac{Ln_2}{\phi_{21}^* - \phi_{20}^*}$ are very large and of order $10^5 - 10^6$. Also, Ln_1 and Ln_2 are large and of order $10^2 - 10^3$ and N_{A_1} and N_{A_2} will not be greater than 10^5 and 10^6 . Using this approximation, the basic solution of the present problem is;

$$\phi_{1b}(z) = z, \phi_{2b}(z) = z, T_b(z) = 1 - z, \text{ and } C_b(z) = 1 - z. \tag{30}$$

Perturbed State

The basic state now considered under the influence of small perturbations. So, the perturbation parameters are

$$\begin{aligned} p &= p_b + p', \phi_1 = \phi_{1b} + \phi'_1, \phi_2 = \phi_{2b} + \phi'_2, \\ \mathbf{u} &= \mathbf{u}(\mathbf{0}) + \mathbf{u}(u', v', w'), T = T_b + T', C = C_b + C', \\ \mathbf{H} &= \mathbf{H}_b + \mathbf{H}'(H'_x, H'_y, H'_z). \end{aligned}$$

The resultant linear governing equations then become:-

$$\nabla \cdot \mathbf{u}' = 0, \tag{31}$$

$$\nabla \cdot \mathbf{H}' = 0, \tag{32}$$

$$\begin{aligned} \frac{1}{Pr} \frac{\partial \mathbf{u}'}{\partial t} = QPm \frac{\partial H'_z}{\partial z} - \nabla p' + \nabla^2 \mathbf{u}' - Rn_1 \phi'_1 \hat{e}_z - Rn_2 \phi'_2 \hat{e}_z \\ + Ra T' \hat{e}_z + \frac{Rs}{Le} C' \hat{e}_z, \end{aligned} \tag{33}$$

$$\frac{\partial H'_z}{\partial t} - Pm \nabla^2 H'_z = \frac{\partial w'}{\partial z}, \tag{34}$$

$$\begin{aligned} \frac{\partial T'}{\partial t} - w' = \nabla^2 T' + \frac{N_{B_1}}{Ln_1} \left(\frac{\partial T'}{\partial z} - \frac{\partial \phi'_1}{\partial z} \right) - \frac{2N_{A_1} N_{B_1}}{Ln_1} \frac{\partial T'}{\partial z} \\ + \frac{N_{B_2}}{Ln_2} \left(\frac{\partial T'}{\partial z} - \frac{\partial \phi'_2}{\partial z} \right) - \frac{2N_{A_2} N_{B_2}}{Ln_2} \frac{\partial T'}{\partial z}, \end{aligned} \tag{35}$$

$$\frac{\partial C'}{\partial t} - w' = \frac{1}{Le} \nabla^2 C', \tag{36}$$

$$\frac{\partial \phi'_1}{\partial t} + w' = \frac{1}{Ln_1} \nabla^2 \phi'_1 + \frac{N_{A_1}}{Ln_1} \nabla^2 T', \tag{37}$$

$$\frac{\partial \phi'_2}{\partial t} + w' = \frac{1}{Ln_2} \nabla^2 \phi'_2 + \frac{N_{A_2}}{Ln_2} \nabla^2 T'. \tag{38}$$

The conditions imposed on the boundaries are

$$\begin{aligned} w' = 0, \frac{\partial w'}{\partial z} + \lambda_1 \frac{d^2 w'}{dz^2} = 0, \phi'_1 = 0, \phi'_2 = 0, \\ T' = 0, C' = 0, \frac{\partial H'_z}{\partial z} = 0 \text{ at } z = 0, \end{aligned} \tag{39}$$

$$\begin{aligned}
 w' = 0, \frac{\partial w'}{\partial z} - \lambda_2 \frac{d^2 w'}{dz^2} = 0, \phi_1' = 0, \phi_2' = 0, \\
 T' = 0, C' = 0, \frac{\partial H_z'}{\partial z} = 0 \text{ at } z = 1.
 \end{aligned}
 \tag{40}$$

The parameter Rm represents the pressure gradient in static state. The parameters $Rn, N_{A1}, N_{A2}, N_{B1}$ and N_{B2} do not appear in the equation for regular binary fluid.

After eliminating p' from the above equations, we obtain:-

$$\begin{aligned}
 \frac{1}{Pr} \frac{\partial}{\partial t} \nabla^2 w' = QPm \frac{\partial(\nabla^2 H_z')}{\partial z} + \nabla^4 w' - Rn_1 \nabla_H^2 \phi_1' \\
 - Rn_2 \nabla_H^2 \phi_2' + Ra \nabla_H^2 T' + \frac{Rs}{Le} \nabla_H^2 C'.
 \end{aligned}
 \tag{41}$$

Combining Eqn. (34) and (41), we get

$$\begin{aligned}
 \left(\frac{\partial}{\partial t} - Pm \nabla^2 \right) \left[\frac{1}{Pr} \frac{\partial}{\partial t} \nabla^2 w' - \nabla^4 w' + Rn_1 \nabla_H^2 \phi_1' + Rn_2 \nabla_H^2 \phi_2' \right. \\
 \left. - Ra \nabla_H^2 T' - \frac{Rs}{Le} \nabla_H^2 C' \right] + QPm \nabla^2 \frac{\partial^2 w'}{\partial z^2} = 0.
 \end{aligned}
 \tag{42}$$

The differential Eqn. (35)-(38) with (42) along with boundary conditions (39) and (40) comprise a linear BVP.

Now to analyse the perturbations into normal modes, we take

$$\begin{aligned}
 [w', \phi_1', \phi_2', T', C'] = [W(z), \Phi_1(z), \Phi_2(z), \Theta(z), \\
 \Gamma(z)] \exp\{ik_x x + ik_y y + nt\}.
 \end{aligned}
 \tag{43}$$

Here, the wave numbers in x direction, y direction are k_x and k_y respectively while $k = (k_x^2 + k_y^2)^{\frac{1}{2}}$. Also, n (complex) is the frequency. Using Eqn. (43) in Eqn. (35)-(38) and (42), we get

$$\begin{aligned}
 \frac{n}{Pr} (D^2 - k^2) W = \frac{QPm(D^2 - k^2) D^2 W}{(n - Pm(D^2 - k^2))} + (D^2 - k^2)^2 W + Rn_1 k^2 \Phi_1 \\
 + Rn_2 k^2 \Phi_2 - Rak^2 \Theta - \frac{Rsk^2}{Le} \Gamma,
 \end{aligned}
 \tag{44}$$

$$\begin{aligned}
 W + \left(D^2 - k^2 - n + \frac{N_{B1}}{Ln_1} D - \frac{2N_{A1} N_{B1}}{Ln_1} D + \frac{N_{B2}}{Ln_2} D \right. \\
 \left. - \frac{2N_{A2} N_{B2}}{Ln_2} D \right) \Theta - \frac{N_{B1}}{Ln_1} D \Phi_1 - \frac{N_{B2}}{Ln_2} D \Phi_2 = 0,
 \end{aligned}
 \tag{45}$$

$$W - \left(n - \frac{1}{Le} (D^2 - k^2) \right) \Gamma = 0,
 \tag{46}$$

$$W - \frac{N_{A1}}{Ln_1} (D^2 - k^2) \Theta - \left(\frac{1}{Ln_1} (D^2 - k^2) - n \right) \Phi_1 = 0,
 \tag{47}$$

$$W - \frac{N_{A2}}{Ln_2} (D^2 - k^2) \Theta - \left(\frac{1}{Ln_2} (D^2 - k^2) - n \right) \Phi_2 = 0.
 \tag{48}$$

To study the linear stability analysis, the corresponding boundary conditions for Free-Free boundaries are:-

$$W = 0, D^2 W = 0, \Phi_1 = 0, \Phi_2 = 0, \Theta = 0, \Gamma = 0 \text{ at } z = 0, 1.
 \tag{49}$$

And for Rigid-Rigid boundaries:-

$$W = 0, DW = 0, \Phi_1 = 0, \Phi_2 = 0, \Theta = 0, \Gamma = 0 \text{ at } z = 0, 1.
 \tag{50}$$

A COMPARATIVE STUDY

We solve the aforementioned eigenvalue problem under various boundary conditions. For every boundary condition in the stationary case (n=0), we compare the outcomes. The aforementioned set of equations has exact solutions for non-realistic boundary conditions (F/F), while numerical solutions are obtained for realistic boundary conditions (R/R, F/R, and R/F).

Realistic Boundary Conditions

In this case, the eigenvalue problem for R/R boundary conditions

$$W = 0, DW = 0, \Phi_1 = 0, \Phi_2 = 0, \Theta = 0, \Gamma = 0 \text{ at } z = 0, 1,
 \tag{51}$$

R/F boundary conditions

$$W = 0, DW = 0, \Phi_1 = 0, \Phi_2 = 0, \Theta = 0, \Gamma = 0 \text{ at } z = 0,
 \tag{52}$$

$$W = 0, D^2 W = 0, \Phi_1 = 0, \Phi_2 = 0, \Theta = 0, \Gamma = 0 \text{ at } z = 1,
 \tag{53}$$

and F/R boundary conditions

$$W = 0, D^2 W = 0, \Phi_1 = 0, \Phi_2 = 0, \Theta = 0, \Gamma = 0 \text{ at } z = 0,
 \tag{54}$$

$$W = 0, DW = 0, \Phi_1 = 0, \Phi_2 = 0, \Theta = 0, \Gamma = 0 \text{ at } z = 1,
 \tag{55}$$

are solved. For the three types of boundary conditions mentioned above, we solve the associated eigenvalue problem using the Galerkin technique. The test (weighted) functions in this method are identical to the base (trial) functions. Initially, the variables are written as linear combination of basis functions as:-

$$\begin{aligned}
 W = \sum_{i=1}^n A_i W_i, \Theta = \sum_{i=1}^n B_i \Theta_i, \Gamma = \sum_{i=1}^n C_i \Gamma_i, \\
 \Phi_1 = \sum_{i=1}^n D_i \Phi_{1i}, \Phi_2 = \sum_{i=1}^n E_i \Phi_{2i},
 \end{aligned}
 \tag{56}$$

where A_i, B_i, C_i, D_i and E_i are constants and the basis function $W_i, \Theta_i, \Gamma_i, \Phi_{1i}, \Phi_{2i}$, are represented by power series satisfy the corresponding boundary conditions. Substituting Eqn. (56) into (44)-(48), multiplying the resulting equations by $W_j(z), \Theta_j(z), \Gamma_j(z), \Phi_{1j}(z)$, and $\Phi_{2j}(z)$, performing the integration by parts with respect to z between z = 0 and z = 1 and using the boundary conditions, leads to the following system of linear homogeneous algebraic equations

$$G_{ji} A_i + H_{ji} B_i + I_{ji} C_i + J_{ji} D_i + K_{ji} E_i = 0,
 \tag{57}$$

$$L_{ji} A_i + M_{ji} B_i + N_{ji} D_i + O_{ji} E_i = 0,
 \tag{58}$$

$$P_{ji}A_i + Q_{ji}C_i = 0, \tag{59}$$

$$R_{ji}A_i + S_{ji}B_i + T_{ji}D_i = 0, \tag{60}$$

$$U_{ji}A_i + V_{ji}B_i + Y_{ji}E_i = 0, \tag{61}$$

where,

$$G_{ji} = -(QPmk^2 + 3Pmk^4)\langle DW_j, DW_i \rangle - (QPm + 3Pmk^2)\langle D^2W_j, D^2W_i \rangle - Pm\langle D^3W_j, D^3W_i \rangle - Pmk^6\langle W_j, W_i \rangle,$$

$$H_{ji} = (RaPmk^4)\langle W_j, \theta_i \rangle + (RaPmk^2)\langle DW_j, D\theta_i \rangle,$$

$$I_{ji} = \frac{PmRsk^4}{Le}\langle W_j, \Gamma_i \rangle + \frac{PmRsk^2}{Le}\langle DW_j, D\Gamma_i \rangle$$

$$J_{ji} = PmRn_1k^4\langle W_j, \Phi_{1i} \rangle - PmRn_1k^2\langle DW_j, D\Phi_{2i} \rangle,$$

$$K_{ji} = -PmRn_2k^4\langle W_j, \Phi_{2i} \rangle - PmRn_2k^2\langle DW_j, D\Phi_{2i} \rangle,$$

$$L_{ji} = \langle \theta_j, W_i \rangle,$$

$$M_{ji} = -\left(\frac{N_{B1}}{Ln_1} - \frac{2N_{A1}N_{B1}}{Ln_1} + \frac{N_{B2}}{Ln_2} - \frac{2N_{A2}N_{B2}}{Ln_2}\right) [-\langle D\theta_j, D\theta_i \rangle - k^2\langle \theta_j, \theta_i \rangle + \langle \theta_j, D\theta_i \rangle],$$

$$N_{ji} = -\frac{N_{B1}}{Ln_1}\langle \theta_j, D\Phi_{1i} \rangle, O_{ji} = -\frac{N_{B2}}{Ln_2}\langle \theta_j, D\Phi_{2i} \rangle,$$

$$P_{ji} = \langle \Gamma_j, W_i \rangle, Q_{ji} = -\frac{k^2}{Le}\langle \Gamma_j, \Gamma_i \rangle - \frac{1}{Le}\langle D\Gamma_j, D\Gamma_i \rangle,$$

$$R_{ji} = \langle \Phi_{1j}, W_i \rangle, S_{ji} = \frac{N_{A1}}{Ln_1}\langle D\Phi_{1j}, D\theta_{1i} \rangle + \frac{N_{A1}k^2}{Ln_1}\langle \Phi_{1j}, \theta_i \rangle,$$

$$T_{ji} = \frac{1}{Ln_1}\langle D\Phi_{1j}, D\Phi_{1i} \rangle + \frac{k^2}{Ln_1}\langle \Phi_{1j}, \Phi_{1i} \rangle,$$

$$U_{ji} = \langle \Phi_{2j}, W_i \rangle, V_{ji} = \frac{N_{A2}}{Ln_2}\langle D\Phi_{2j}, D\theta_{2i} \rangle + \frac{N_{A2}k^2}{Ln_2}\langle \Phi_{2j}, \theta_i \rangle,$$

$$Y_{ji} = \frac{1}{Ln_2}\langle D\Phi_{2j}, D\Phi_{2i} \rangle + \frac{k^2}{Ln_2}\langle \Phi_{2j}, \Phi_{2i} \rangle.$$

Here the inner product $\langle \dots \rangle$ is defined as $\langle \dots \rangle = \int_0^1 (\dots) dz$.

The above set of homogeneous algebraic equations can have a non-trivial solution if and only if

$$\begin{bmatrix} G_{ji} & H_{ji} & I_{ji} & J_{ji} & K_{ji} \\ L_{ji} & M_{ji} & 0 & N_{ji} & O_{ji} \\ P_{ji} & 0 & Q_{ji} & 0 & 0 \\ R_{ji} & S_{ji} & 0 & T_{ji} & 0 \\ U_{ji} & V_{ji} & 0 & 0 & Y_{ji} \end{bmatrix} = 0. \tag{62}$$

For R/R boundaries, trial functions are:-

$$W_i = z^{i+1} - 2z^{i+2} + z^{i+3}, \theta_i = \Gamma_i = \Phi_{1i} = \Phi_{2i} = z^i - z^{i+1}, \tag{63}$$

for R/F boundaries, trial functions are:-

$$W_i = 2z^{i+3} + 3z^{i+1} - 5z^{i+2}, \theta_i = \Gamma_i = \Phi_{1i} = \Phi_{2i} = z^i - z^{i+1}, \tag{64}$$

and for F/R boundaries conditions, trial functions are:-

$$W_i = z^{i+4} + z^{i+2} - 2z^{i+3}, \theta_i = \Gamma_i = \Phi_{1i} = \Phi_{2i} = z^i - z^{i+1}. \tag{65}$$

Here $(i=1,2,3\dots n)$.

From a rigorous numerical experiment, it has been found that the order of the polynomial, $n = 5$ is sufficient to reach the required accuracy, which is shown in Table 1.

Non Realistic Boundary Conditions

We take the solution of Eqn. (44)-(48) satisfying the boundary condition for Free-Free (F/F) case:-

$$W = W_0 \text{Sinn}\pi z, \theta = \theta_0 \text{Sinn}\pi z, \Gamma = \Gamma_0 \text{Sinn}\pi z, \Phi_1 = \Phi_{10} \text{Sinn}\pi z, \Phi_2 = \Phi_{20} \text{Sinn}\pi z. \tag{66}$$

Substituting Eqn. (66) in the above equations, we get the matrix equation as:-

$$[a_{ij}][W_0 \ \theta_0 \ \Gamma_0 \ \Phi_{10} \ \Phi_{20}]^T = 0. \tag{67}$$

Here $\delta = \pi^2 + k^2$ and $a_{11} = \delta^2 + \frac{n\delta}{Pr} + \frac{QPm\delta\pi^2}{n+Pm\delta}$, $a_{12} = -Rak^2$, $a_{13} = -\frac{Rsk^2}{Le}$, $a_{14} = Rn_1k^2$, $a_{15} = Rn_2k^2$, $a_{21} = 1$, $a_{22} = -(\delta + n)$, $a_{23} = 0$, $a_{24} = 0$, $a_{25} = 0$, $a_{31} = 1$, $a_{32} = 0$, $a_{33} = -\left(n + \frac{\delta}{Le}\right)$, $a_{34} = 0$, $a_{35} = 0$, $a_{41} = 1$, $a_{42} = \frac{N_{A1}}{Ln_1}\delta$, $a_{43} = 0$, $a_{44} = n + \frac{\delta}{Ln_1}$, $a_{45} = 0$, $a_{51} = 1$, $a_{52} = \frac{N_{A2}}{Ln_2}\delta$, $a_{53} = 0$, $a_{54} = 0$, $a_{55} = n + \frac{\delta}{Ln_2}$.

Table 1. Comparison of results for different orders of Galerkin approximation for $Ln_2=100$ for different values Q.

	n=2		n=3		n=4		n=5	
	Ra_T^c	a^c	Ra_T^c	a^c	Ra_T^c	a^c	Ra_T^c	a^c
Q=0	53.5797	1.42	53.5797	1.42	53.5792	1.41	53.5792	1.41
Q=10	213.5874	1.71	213.5874	1.71	213.5872	1.71	213.5872	1.71
Q=20	361.5517	1.76	361.5513	1.75	361.5513	1.75	361.5513	1.75
Q=30	503.9994	1.83	503.9994	1.83	503.9994	1.83	503.9994	1.83

The non-trivial solution of the above homogeneous system of equations require that

$$Ra = \left(\delta^2 + \frac{n\delta}{Pr} + \frac{Q\text{Pm}\delta\pi^2}{n+\text{Pm}\delta} \right) \left(\frac{n+\delta}{k^2} \right) - \frac{Rs}{Le} \left(\frac{n+\delta}{n+\frac{\delta}{Le}} \right) - \frac{(\text{Ln}_1(n+\delta)+\delta N_{A1})}{n\text{Ln}_1+\delta} \text{Rn}_1 - \frac{(\text{Ln}_2(n+\delta)+\delta N_{A2})}{n\text{Ln}_2+\delta} \text{Rn}_2. \quad (68)$$

Non Oscillatory Convection

When $n = 0$. The stationary Rayleigh number is given by:-

$$Ra^{st} = (\delta^2 + Q\pi^2) \left(\frac{\delta}{k^2} \right) - Rs - \frac{(\text{Ln}_1\delta+\delta N_{A1})}{\delta} \text{Rn}_1 - \frac{(\text{Ln}_2\delta+\delta N_{A2})}{\delta} \text{Rn}_2, \quad (69)$$

After neglecting the solute Rayleigh number (Rs) and Chandrashekhkar number (Q), Eqn. (69) gives

$$Ra^{st} = \frac{\delta^3}{k^2} - (\text{Ln}_1 + N_{A1})\text{Rn}_1 - (\text{Ln}_2 + N_{A2})\text{Rn}_2. \quad (70)$$

The same result has been obtained by [33].

RESULTS AND DISCUSSION

The effect of the main controlling parameters on the onset of convection in hybrid nanofluid is examined with the objective of understanding the control over convection. It has been observed that the thermal Rayleigh numbers of hybrid nanofluid are unaffected by the modified particle density parameter increment for non-oscillatory convection.

Linear Stability Analysis

Linear stability analysis is divided into one subsection: It is dedicated to a comparative study of stationary or non-oscillatory cases for different boundary conditions.

Comparative Study (Non-Oscillatory Case)

Here, we have plotted the graphs for the main controlling parameters, such as Chandrashekhkar number (Q), which represents the magnetic field effect, thermo-nanofluid Lewis numbers (Ln_1, Ln_2), nanoparticle concentration numbers (Rn_1, Rn_2) in the (Rs, Ra^c) plane for Free-Free(F/F), Free-Rigid (F/R), Rigid-Free (R/F) and Rigid-Rigid(R/R) boundaries.

The effect of the Chandrashekhkar number (Q) is depicted in Figure 2 for various boundaries in the (Rs, Ra^c) plane when other parameters have fixed values. In

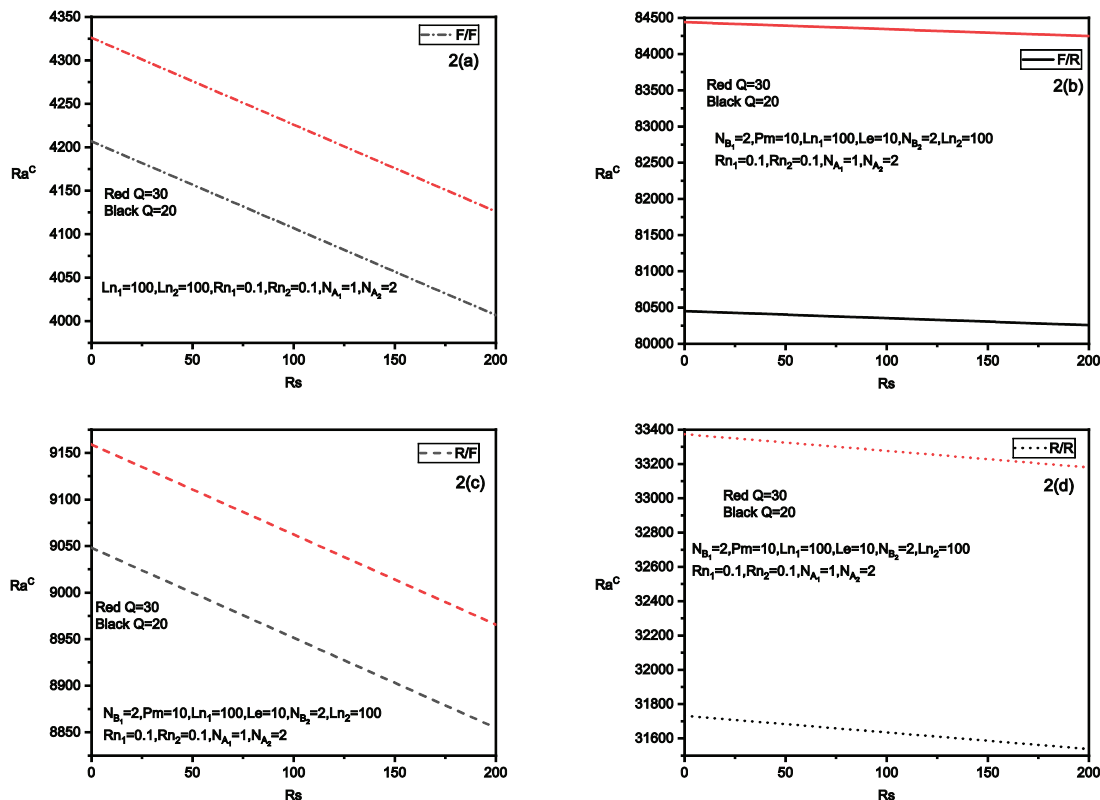


Figure 2. Variation of Ra^c as function for different values of (Q) on (Rs, Ra^c) plane.

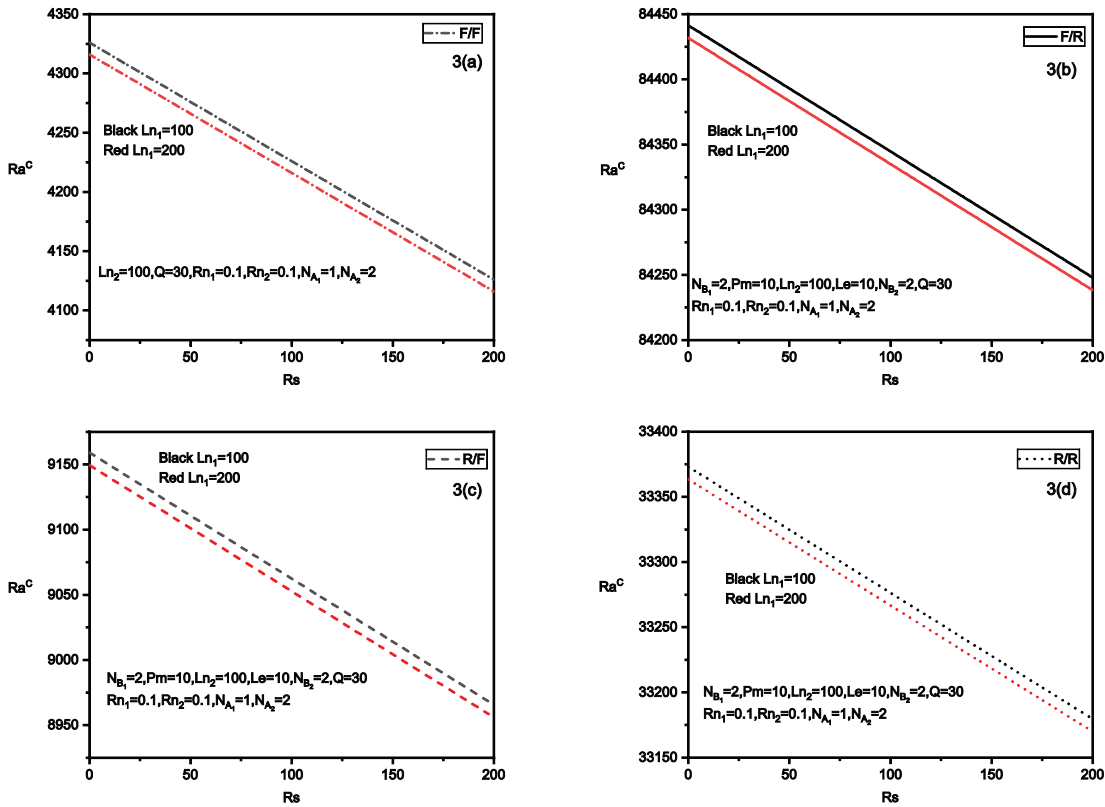


Figure 3. Variation of Ra^C as function for different values of (Ln_1) on (Rs, Ra^C) plane.

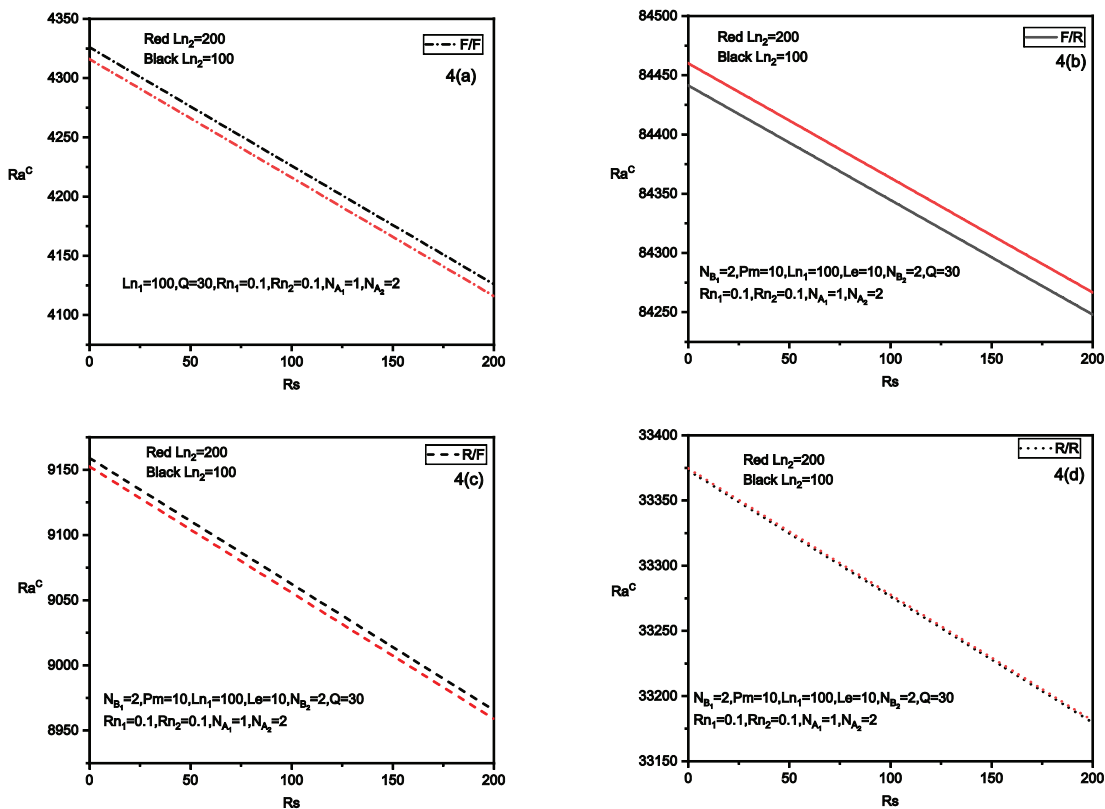


Figure 4. Variation of Ra^C as function for different values of (Ln_2) on (Rs, Ra^C) plane.

each of the four cases, F/F, F/R, R/F, and R/R, the stability of the system increases as the value of Q increases. This shows that the system stabilizes with an increasing value of Q , indicating the onset of convection delay. This phenomenon can be explained by the fact that viscosity is introduced into the fluid, and convection distorts the magnetic lines when a magnetic field penetrates the medium with a significant degree of strength. Consequently, the development of disturbances is impeded by these magnetic lines, delaying the onset of instability. Also from the graphs in Figure 2, one can conclude that the stability of the system is most dominant for F/R boundaries and least for F/F boundaries. This result is similar to the findings of [34].

Figure 3 illustrates how the stability of a system under different boundaries is affected by the change in the value of the thermo-nanofluid Lewis number (Ln_1). The stability of the system reduces when the value of Ln_1 increases in all scenarios, i.e., F/F, F/R, R/F, and R/R. The stability of the system is described as: $F/R > R/R > F/R > F/F$ i.e. the system is most stable at F/R and least stable at F/F boundaries.

The impact of the thermo-nanofluid Lewis number (Ln_2) for different boundaries is depicted in Figure 4. We observed a complex nature with the change in the value of Ln_2 . As Ln_2 increases, the stability of the system falls in the cases of F/F and R/F, whereas it increases for the F/R and R/R boundaries. Stability is greatest for F/R boundaries and lowest for F/F boundaries. Similar results were obtained by [33].

Figure 5 shows the behavior of stability criteria for different types of boundaries for changes in the value of nanoparticle concentration number (Rn_1). In all cases, i.e., F/F, F/R, R/F, and R/R, the system's stability decreases with an increasing value of Rn_1 .

Figure 6 depicts the impact of nanoparticle concentration number (Rn_2) on the stability of the system for all four boundaries combinations. In all cases i.e. F/F, F/R, R/F, R/R, stability of the system decreases as the value of Rn_2 increases. The behavior of nanoparticles concentration Rayleigh numbers is clear and consistent with what Chand and Rana reported [35, 36]. In general, if both Rn_1 and Rn_2 take the negative values, the hybrid nanofluid layer will be more stable.

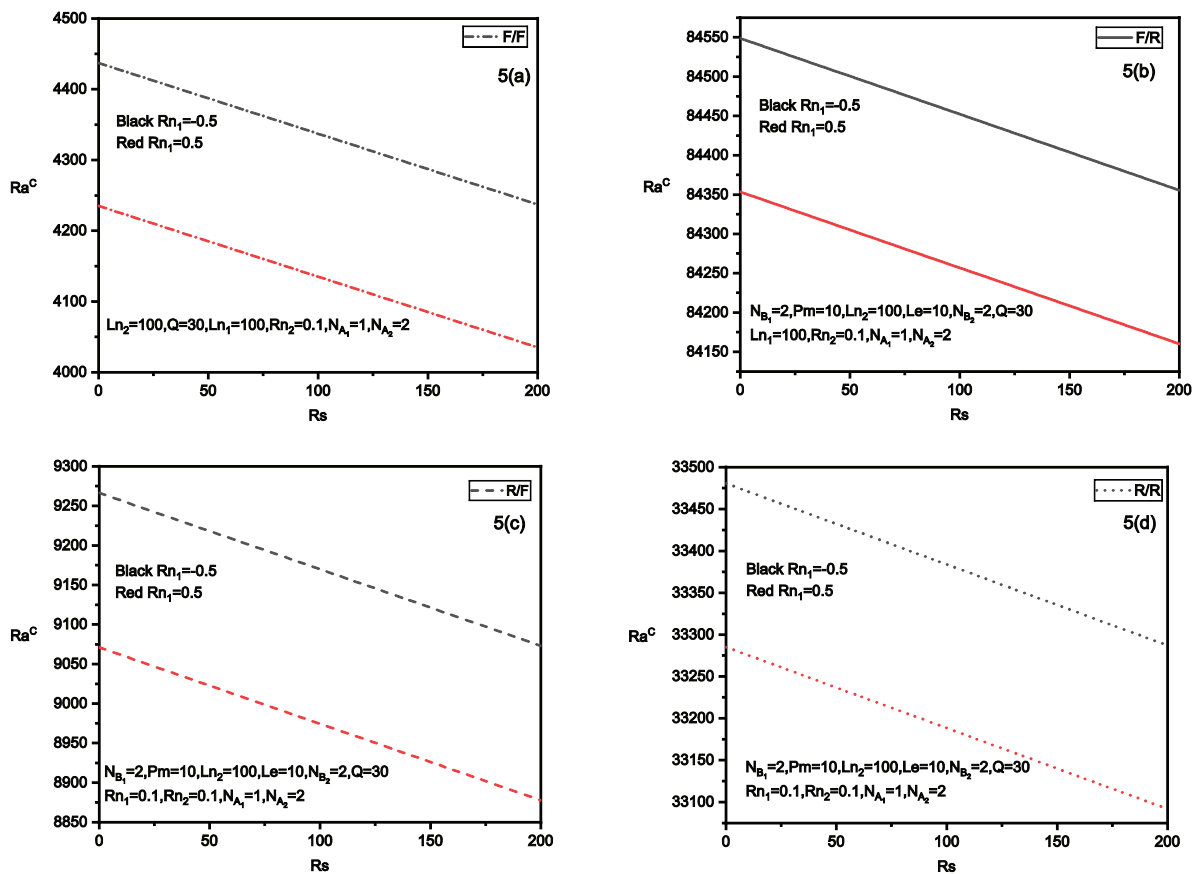


Figure 5. Variation of Ra^c as function for different values of (Rn_1) on (Rs, Ra^c) plane.

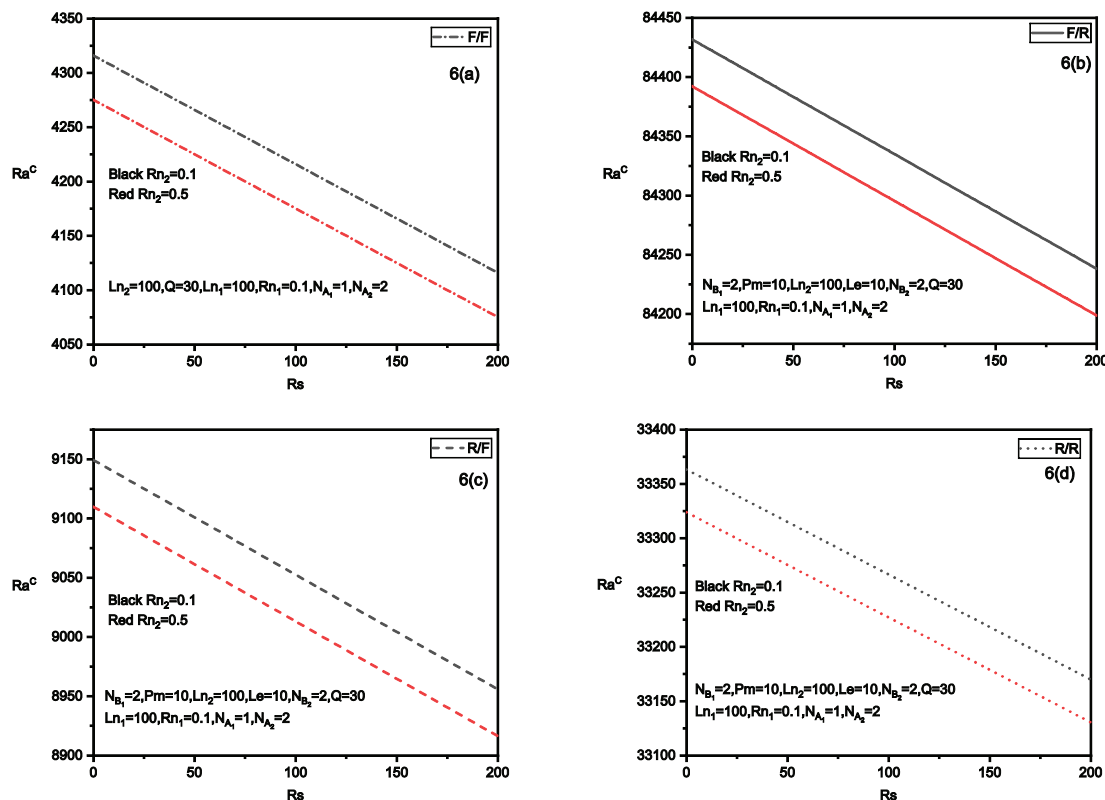


Figure 6. Variation of Ra^c as function for different values of (Rn_2) on (Rs, Ra^c) plane.

CONCLUSION

We have tried to understand how hybrid nanofluids and magnetic fields can influence the onset of double diffusive convection. We carried out a comparison analysis based on various boundary conditions using linear stability analysis. Four different velocity boundary conditions, namely R/R, R/F, F/R, and F/F have been analyzed. The Galerkin technique is used to solve the eigenvalue problem for the R/R, R/F, and F/R boundaries, whereas exact solutions are obtained for the F/F boundaries. In the non-oscillatory condition, we examine the outcomes among four boundary conditions.

The conclusions are as follows:-

- For each of the four boundary surfaces, the stability of the system rises as Q grows.
- With rising values of Ln_1 , Rn_1 , and Rn_2 for every boundary, the system's stability diminishes.
- With an increasing value of Ln_2 , an intriguing stability phenomenon in the system was found. With an increasing value of Ln_2 , the system becomes unstable in two combinations (F/F and R/F), but it has the opposite effect on the other two combinations (R/R and F/R).
- Furthermore, based on the studies mentioned above, we can deduce that the system's stability is stated in the following order: $F/R > R/R > R/F > F/F$. This means that the system is most stable for F/R boundaries and least stable for F/F boundaries.

ACKNOWLEDGEMENTS

Author Monal Bharty gratefully acknowledges the financial assistance from Central university of Jharkhand as a research fellowship.

AUTHORSHIP CONTRIBUTIONS

Authors equally contributed to this work.

DATA AVAILABILITY STATEMENT

The authors confirm that the data that supports the findings of this study are available within the article. Raw data that support the finding of this study are available from the corresponding author, upon reasonable request.

CONFLICT OF INTEREST

The author declared no potential conflicts of interest with respect to the research, authorship, and/or publication of this article.

ETHICS

There are no ethical issues with the publication of this manuscript.

NOMENCLATURE

a	Wave number, m^{-1}
c	Specific heat of nanofluid, $kJ / kg \text{ } ^\circ C$
C	Concentration of the solute, mol/m^3
C_0	Upper layer concentration,
D_{B1}, D_{B2}	Brownian diffusion coefficients of two nanoparticles, m^2/s
D_{T1}, D_{T2}	Thermophoretic diffusion coefficients
D_s	Solutal diffusivity, m^2/s
g	Acceleration due to gravity, m/s^2
H	Magnetic field, T
Le	Concentration based Lewis number
Ln_1, Ln_2	Themo-nanofluid Lewis number
n	Growth rate
N_{A1}, N_{A2}	Modified diffusivity ratio
N_{B1}, N_{B2}	Modified particle density increment
Pr	Prandtl number
T	Temperature, K
T_0	Temperature of upper layer
Ra	Temperature based Rayleigh number
Rs	Concentration based Rayleigh number
Rm	Density based Rayleigh number

Greek symbols

α_f	Fluid's thermal diffusivity, m^2/s
β_T	Temperature based volumetric coefficient, K^{-1}
β_C	Solutal Volumetric fraction
κ	Thermal conductivity of nanofluid, $W / m \text{ } ^\circ C$
μ	The viscosity of the nanofluid, Pa s
ϕ_1^*, ϕ_2^*	Nanoparticle volume fraction
ρ_{p1}, ρ_{p2}	Nanoparticles mass densities, kg/m^3

REFERENCES

- [1] Tzou DY. Instability of Nanofluids in Natural Convection. ASME J Heat Transf 2008;130:072401(1–9). [CrossRef]
- [2] Choi US, Eastman JA. Enhancing thermal conductivity of fluid with nanoparticles. ASME IMECE 1995;12–17 November:1–8 San Francisco, CA.
- [3] Hwang Y, Lee JK, Lee CH, Jung YM, Cheong SI, Lee CG. Stability and thermal conductivity characteristics of nanofluids. Thermochim Acta 2007;455:70–74. [CrossRef]
- [4] Botha SS, Ndungu P, Bladergroen BJ. Physicochemical properties of oil-based nanofluids containing hybrid structures of silver nanoparticles supported on silica. Ind Eng Chem Res 2011;50:3071–3077. [CrossRef]
- [5] Murshed SM, Tan SH, Nguyen NT. Temperature dependence of interfacial properties and viscosity of nanofluids for droplet-based microfluidics. J Phys D Appl Phys 2008;41:085502. [CrossRef]
- [6] Chen L, Xie H. Silicon oil based multiwalled carbon nanotubes nanofluid with optimized thermal conductivity enhancement. Colloids Surf 2009;352:136–140. [CrossRef]
- [7] Garoosi F, Garoosi S, Hooman K. Numerical simulation of natural convection and mixed convection of the nanofluid in a square cavity using Buongiorno model. Powder Technol 2014;268:279–292. [CrossRef]
- [8] Garoosi F, Bagheri G, Rashidi MM. Two phase simulation of natural convection and mixed convection of the nanofluid in a square cavity. Powder Technol 2015;275:239–256. [CrossRef]
- [9] Chand R, Rana GC, Hussein AK. Effect of suspended particles on the onset of thermal convection in a nanofluid layer for more realistic boundary conditions. Int J Fluid Mech Res 2015;42:375–390. [CrossRef]
- [10] Rana GC, Chand R, Sharma V. Thermal instability of a Rivlin–Ericksen nanofluid saturated by a Darcy–Brinkman porous medium: a more realistic model. Eng Trans 2016;64:271–286.
- [11] Noureen M, Marwat DNK. Double-diffusive convection: Flow of nanofluid of variable heat capacity inside rectangular and inclined walls. Ain Shams Eng J 2022;14:101889(1–16). [CrossRef]
- [12] Li H, Ha CS, Kim I. Fabrication of carbon nanotube/SiO2 and carbon nanotube/SiO2/Ag nanoparticles hybrids by using plasma treatment. Nanoscale Res Lett 2009;4:1384–1388. [CrossRef]
- [13] Guo S, Dong S, Wang E. Gold/platinum hybrid nanoparticles supported on multiwalled carbon nanotube/silica coaxial nanocables: preparation and application as electrocatalysts for oxygen reduction. J Phys Chem C 2008;112:2389–2393. [CrossRef]
- [14] Ahmad B, Abbas T, Fatima K, Duraihem FZ, Saleem S. Nonlinear flow of hybrid nanofluid with thermal radiation: A numerical investigation. ZAMM 2024;104: e202200228. [CrossRef]
- [15] Pundir SK, Awasthi MK, Kumar V. Double-Diffusive Convection in a Hybrid Nanofluid Layer. J Nanofluids 2022;11:296–304. [CrossRef]
- [16] Pop I, Ingham DB. Convective Heat Transfer: Mathematical and Computational Modeling of Viscous Fluids and Porous Media. Pergamon, Oxford; 2001.
- [17] Bilal S, Shah IA, Khan I, et al. FEM simulations for double diffusive transport mechanism hybrid nano fluid flow in corrugated enclosure by installing uniformly heated and concentrated cylinder. Sci Rep 2024;14:766–782. [CrossRef]
- [18] Sharma J, Gupta U. Double-Diffusive Nanofluid Convection in Porous Medium with Rotation: Darcy-Brinkman Model. Procedia Eng 2015;127:783–790. [CrossRef]
- [19] Pranesh S, Siddheshwar PG, Tarannum S, Yekasi V. Convection in a horizontal layer of water with three diffusing components. SN Appl Sci 2020;2:806. [CrossRef]
- [20] Krishna MV, Bharathi K, Chamkha AJ. Hall's effect on MHD peristaltic flow of Jeffery fluid through porous medium in a vertical stratum. Interfacial Phenom Heat Transf 2018;6:253–268. [CrossRef]

- [21] Krishna MV, Reddy MG, Chamkha AJ. Heat and mass transfer on MHD free convective flow over an infinite nonconducting vertical flat porous plate. *Int J Fluid Mech Res* 2019;46:1–25. [[CrossRef](#)]
- [22] Krishna MV, Chamkha AJ. MHD Peristaltic rotating flow of a couple stress fluid through a porous medium with wall and sleep effect. *Spec Top Rev Porous Media* 2019;10:245–258. [[CrossRef](#)]
- [23] Kandaswamy P, Sundari SM, Nithyadevi N. Magnetoconvection in an enclosure with partially active vertical walls. *Int J Heat Mass Transf* 2008;51:1946–1954. [[CrossRef](#)]
- [24] Nasrin R, Parvin S. Hydromagnetic effect on mixed convection in a lid-driven cavity with sinusoidal corrugated bottom surface. *Int Commun Heat Mass Transf* 2011;38:781–789. [[CrossRef](#)]
- [25] Neeraja A, Devi RLVR, Devika B, Radhika VN, Murthy MK. Effects of viscous dissipation and convective boundary conditions on magnetohydrodynamics flow of casson liquid over a deformable porous channel. *Results Eng* 2019;4:100040. [[CrossRef](#)]
- [26] Nabwey HA, Rashad AM, Mansour MA, Salah T. Magneto-Nanofluid Flow via Mixed Convection Inside E-Shaped Square Chamber. *Symmetry* 2022;14:1159–1175. [[CrossRef](#)]
- [27] Roy NC. MHD natural convection of a hybrid nanofluid in an enclosure with multiple heat sources. *Alex Eng J* 2022;61:1679–1694. [[CrossRef](#)]
- [28] Acharya N. Magnetized hybrid nanofluid flow within a cube fitted with circular cylinder and its different thermal boundary conditions. *J Magn Magn Mater* 2022;564:170167. [[CrossRef](#)]
- [29] Rashad AM, Nafe MA, Eisa DA. Heat variation on MHD Williamson hybrid nanofluid flow with convective boundary condition and Ohmic heating in a porous material. *Sci Rep* 2023;13:6071–6085. [[CrossRef](#)]
- [30] Anee MJ, Hasan MF, Siddiqa S, Molla MM. MHD Natural Convection and Sensitivity Analysis of Ethylene Glycol Cu-Al₂O₃ Hybrid Nanofluids in a Chamber with Multiple Heaters: A Numerical Study of Lattice Boltzman Method. *Int J Energy Res* 2024;5521610:1–25. [[CrossRef](#)]
- [31] Wahid NS, Arifin NM, Khashi'ie NS, Pop I. Mixed convection MHD hybrid nanofluid over a shrinking permeable inclined plate with thermal radiation effect. *Alex Eng J* 2023;769–783. [[CrossRef](#)]
- [32] Tzou DY. Instability of Nanofluids in Natural Convection. *Int J Heat Mass Transf* 2008;51:2967–2979. [[CrossRef](#)]
- [33] Kumar V, Awasthi MK. Thermal instability in a horizontal composite nano-liquid layer. *Discover Appl Sci* 2020;2:380. [[CrossRef](#)]
- [34] Bharty M, Srivastava AK, Mahato H. Stability of Magneto Double Diffusive Convection in Couple Stress Liquid with Chemical Reaction. *J Heat Mass Transf Res* 2023;20:171–190.
- [35] Chand R, Rana GC. Thermal instability in a Brinkman porous medium saturated by nanofluid with no nanoparticle flux on the boundaries. *Spec Top Rev Porous Media* 2014;5:277–286. [[CrossRef](#)]
- [36] Chand R, Rana GC. Magneto convection in a layer of nanofluid in a porous medium—a more realistic approach. *J Nanofluids* 2015;4:196–202. [[CrossRef](#)]